RESEARCH ARTICLE

Radiative and Viscous Dissipative Flow of a Chemically Reacting MHD Casson Nanofluid over an Inclined Slippery Stretching Surface with Non-Darcian Medium

Jos Usman Abubakar[1], Timothy Lanre Oyekunle[1], Mojeed Taiwo Akolade[2], Samson Ademola Agunbiade[3], Ruth Blessing Oladeji[1,*] and Thomas Olanrewaju Olotu[1]

[1] Department of Mathematics, University of Ilorin, Ilorin, Nigeria
[2] Department of Computer Science, Lead City University, Ibadan, Nigeria
[3] Department of Basic Sciences, Babcock University, Ilishan-Remo 121103, Nigeria

Abstract

The study of coupled reaction transport in Casson rheology bridges the gap between idealized Newtonian models and practical non-Newtonian fluids, as chemically reacting nanoparticles alter the concentration and thermal behavior of the base fluid. This complexity intensifies when nanoparticles are introduced into conventional refrigerants. This work presents a unified investigation of radiative and viscous dissipative magnetohydrodynamic flow of a chemically reacting Casson nanofluid over an inclined slippery stretching surface embedded in a non-Darcy porous medium. The simultaneous consideration of Casson rheology, nanoparticle-enhanced heat transfer, magnetic control, surface slip, chemical reaction, and inertial porous effects offers a realistic model for high-temperature industrial, biomedical, and energy applications. Using similarity transformations, the governing partial differential equations are reduced to dimensionless coupled nonlinear ordinary differential equations, which are solved via the Legendre collocation technique. Numerical results, presented in tables and graphs, show that velocity and temperature increase with higher radiation parameter, while nanoparticle volume fraction decreases. Temperature rises with increasing Eckert number and heat source parameter. Higher slip parameter reduces temperature, wall shear stress, and near-surface chemical concentration. These findings provide insight for optimizing thermal performance, reaction efficiency, and flow control in complex engineering and bioengineering systems.

Keywords: viscous dissipation, forchheimer effect, casson nanofluid, legendre polynomial.

Submitted: 13 January 2026
Accepted: 18 February 2026
Published: 25 April 2026

Vol. 2, **No.** 2, 2026.
10.62762/JAM.2026.785346

***Corresponding author:**
Ruth Blessing Oladeji
blessingoladeji4@gmail.com

Citation
Abubakar, J. U., Oyekunle, T. L., Akolade, M. T., Agunbiade, S. A., Oladeji, B. R., & Olotu, T. O. (2026). Radiative and Viscous Dissipative Flow of a Chemically Reacting MHD Casson Nanofluid over an Inclined Slippery Stretching Surface with Non-Darcian Medium. *ICCK Journal of Applied Mathematics*, 2(2), 153–165.

Nomenclature

Symbol	Description	Symbol	Description
ω	Casson fluid parameter	Nt	Thermophoresis Parameter
B_0	Constant of magnetic field	Nb	Brownian motion parameter
ρ	Fluid density	Cf_x	Skin friction
H	Magnetic parameter	Ns	Slip constant
τ	Inclination angle	β_t	Thermal expansion coefficient
α	Thermal diffusion factor	D_m	Brownian coefficient
S_r	Soret number	T_0	Temperature slip constant
q	Stretching sheet index parameter	Q_0	Heat source coefficient
π	Casson fluid deformation rate	C_0	Nanoparticle heat capacity ratio
C_p	Specific heat at constant g	λ	Solutal buoyancy parameter
g_x	Velocity slip parameter	γ	Thermal buoyancy parameter
λ_u	Velocity slip	u, v	Velocity components
U_s	Thermal Grashof number	τ_{ij}	Stress tensor
μ	Dynamic viscosity	e_{ij}	Strain tensor rate
K	Thermal conductivity	ξ	Similarity variable
U_f	Surface fluid velocity	R_{ex}	Reynolds number
μ_B	Casson dynamic viscosity	k^*	Absorption constant
D_B	Mass diffusion coefficient	σ^*	Stefan-Boltzmann number
P_x	Yield stress	Q	Heat source/sink
λ_t	Temperature slip parameter	N	Radiation Parameter
κ	Reaction rate parameter	B	Permeability parameter
K_p	Permeability coefficient	E_c	Eckert number
ω_c	Concentration slip parameter	Sc	Schmidt number
F_c	Forchheimer parameter	g	Chemical reaction parameter
G_c	Solutal Grashof number	Pr	Prandtl number
v	Kinematic viscosity	C_f	Forchheimer coefficient
π_c	Casson model critical value		

1 Introduction

Non-Newtonian fluids arise in numerous industrial, biomedical, energy, and environmental applications where Newtonian models are inadequate to describe complex rheological behavior. Unlike Newtonian fluids, whose viscosity remains constant regardless of the applied shear rate, non-Newtonian fluids exhibit shear-dependent viscosity, yield stress, viscoelasticity, or time-dependent deformation. These characteristics make their flow behavior significantly more complicated and require specialized constitutive models for accurate prediction. Among these fluids, the Casson fluid model has gained considerable prominence due to its ability to represent yield stress and viscoplastic characteristics observed in materials such as blood, printing ink, grease, honey, gels, chocolate syrup, and industrial slurries. The presence of yield stress implies that the fluid behaves like an elastic solid until a critical stress threshold is exceeded, after which it flows like a viscous fluid. This dual solid–fluid nature is particularly important in physiological transport and coating processes where flow initiation is not instantaneous. Invariably, the Casson model has been widely used for simulating physiological suspensions and industrial transport processes, as reported by Hussain et al. [1], Nasir et al. [2], and Kiyani et al. [3]. Investigations into boundary-layer Casson fluid flows by Nadeem et al. [4] and Hussanan et al. [5] revealed that Casson rheology substantially modifies momentum transport, leading to reduced velocity distributions compared with Newtonian fluids. This reduction occurs because the effective viscosity increases in low-shear regions, thickening the momentum boundary layer and increasing resistance to motion. When extended to magnetohydrodynamics (MHD) flows, the presence of a transverse magnetic field introduces Lorentz forces that suppress fluid motion while enhancing thermal energy due to Joule heating effects, as demonstrated by Nasir et al. [2]. Physically, the Lorentz force acts opposite to the flow direction, converting kinetic energy into thermal energy, thereby coupling momentum and heat transfer processes. The velocity and temperature profiles increase with buoyancy forces whereas the concentration distributions diminishes as observed by Akolade et al. [6] and Oyekunle et al. [7].

Introducing nanoparticles into conventional base fluids to form nanofluids has been recognized as an effective approach to enhance thermal conductivity and convective heat transfer. Nanoparticles possess significantly higher thermal conductivity than base fluids, and their dispersion creates additional microscopic heat transport pathways. Studies by Aroloye et al. [8] and Varatharaj et al. [9] confirmed that the combination of Casson nanofluid and thermal enhancement effects of nanoparticles increases heat transfer in biomedical heat exchanger, solar-thermal systems, microelectronics cooling and chemical processing applications. In such systems, improved thermal transport reduces temperature gradients, prevents overheating, and enhances system longevity. The fundamental nanoparticle transport mechanisms, Brownian motion and thermophoresis were systematically formulated by Buongiorno [10], providing the foundation for modern nanofluid modeling. Brownian motion represents random particle movement due to molecular collisions, while thermophoresis describes particle migration from hot to cold regions; both mechanisms strongly influence nanoparticle distribution and, consequently, local thermal conductivity. This framework was later extended to buoyancy-driven convection by Kuznetsov et al. [11], who showed that nanoparticle dynamics substantially modify thermal and solutal boundary layers. The altered particle concentration fields directly affect density gradients, thereby modifying buoyancy forces and flow stability. Further advancements in nanofluid dynamics have explored the synergistic effects of hybrid compositions. For instance, Gangadharaiah et al. [12] investigated penetrative convection in dual-component hybrid nanofluids, noting that nanoparticle distribution significantly dictates the stability of the system. Expansion on these complex architectures, Yusuf et al. [13] recently conducted a sensitivity analysis on regularized curved solar panels utilizing non-Newtonian quaternary hybrid nanofluids. Their findings demonstrated that the use of a sodium alginate-based quaternary system can enhance thermal efficiency by approximately 37% compared to traditional water-based fluids, particularly when utilizing variable heat absorption to mitigate overheating in high-irradiance regions. These results highlight the growing importance of multi-component nanofluids in next-generation renewable energy systems.

Casson nanofluid flows over stretching and shrinking surfaces under various physical effects have been widely explored in the literature. Stretching surfaces are idealized representations of extrusion, polymer sheet production, glass-fiber manufacturing, and coating processes, where surface motion directly controls boundary-layer development. Kiyani et al. [3], Umar et al. [14], and Islam et al. [15] examined the combined influences of velocity slip, thermal radiation, and chemical reactions, reporting notable enhancements in heat transfer characteristics. Velocity slip arises in micro- and nano-scale flows or rarefied environments where the no-slip condition breaks down, altering shear stress and heat transfer near the wall. Others considered the introduction of thermal radiation, heat source/sink and slip condition into Casson nanofluid models, consistently noticing an increased heat transfer [16, 17]. Recent analytical investigations by Manjunatha et al. [18] have underscored the impact of radiation and magnetic fields on rotating nanofluid systems. Furthermore, the interplay between surface reactions and fluid dynamics has become a focal point of recent study; Yusuf et al. [19] investigated the coupling of non-thermal plasma and photocatalytic surface reactions in ZnO-Au/water hybrid nanofluids. Their study highlighted how non-spherical particle morphologies and plasma-generated species synergistically enhance mass and heat transfer rates, which is critical for accelerating photocatalytic degradation and optimizing fluid momentum near catalytic surfaces. Such multiphysics coupling illustrates how chemical, electromagnetic, and hydrodynamic processes can no longer be studied independently in advanced thermal systems. The inclusion of nanoparticles and slip conditions was further shown to improve thermal efficiency in biomedical and engineering systems, as demonstrated by Elelamy et al. [20]. More recent studies involving hybrid and ternary nanofluids revealed further improvements in thermal transport under radiative and MHD effects, as discussed by Ishaq et al. [21] and Usman et al. [22].

In high-temperature and high-shear environments, viscous dissipation and thermal radiation play dominant roles in thermal transport processes. Viscous dissipation represents the conversion of mechanical energy into internal energy due to fluid friction, which becomes significant when velocities or viscosities are high. Applications such as lubrication systems, polymer processing, geothermal engineering, and microfluidic heating are particularly sensitive to frictional heating effects. Early work of Gebhart [23] established that viscous dissipation significantly thickens thermal boundary layers at high Eckert numbers. Subsequent investigations confirmed that viscous dissipation alters temperature distributions and can reduce heat transfer efficiency, as reported by Muduly et al. [24] and Basha [25]. Thermal radiation also plays important role in gas turbines, thermal insulation, nuclear reactor, combustion chamber and solar collectors. Their inclusion in the thermal transport studies of non-Newtonian fluid is critical, as shown by Aziz [26] and Dero et al. [27]. Radiative heat transfer becomes dominant when temperature differences are large, making the Rosseland approximation commonly employed in boundary-layer analysis. Moreover, the presence of internal heat sources significantly alters convective stability; Manjunatha et al. [28] explored these effects in composite layers with non-uniform temperature gradients, finding that the interplay between Marangoni effects and heat generation is vital for predicting thermal performance.

In many realistic industrial and geophysical configurations, fluid motion occurs within porous media, where inertial effects become significant. Porous structures such as packed beds, geothermal reservoirs, biological tissues, and catalytic reactors introduce resistance that alters flow structure and heat transport. Under such circumstances, the classical Darcy model becomes insufficient, requiring the incorporation of Forchheimer (non-Darcy) effects to account for form drag and permeability resistance. Cui et al. [29] and Bejawada et al. [30] have emphasized the importance of non-Darcy resistance in Casson and nanofluid flows. The complexity of these systems increases when considering viscosity variations and couple-stress effects. Gangadharaiah et al. [31] demonstrated that exponential viscosity models and through-flow parameters are crucial for suppressing convective instabilities in porous structures. Additionally, Narayanappa et al. [32] highlighted the influence of Local Thermal Non-Equilibrium (LTNE) and various temperature gradient profiles on magneto-convective stability. Furthermore, several practical systems operate on inclined surfaces, where gravitational components modify buoyancy forces. Nield et al. [33] provide theoretical insights into inclination effects, while numerical studies demonstrated that surface inclination suppresses velocity but enhances heat transfer in Casson nanofluid systems, as reported by Choudhary et al. [34] and Kumari et al. [35]. Comprehensive reviews on the mathematical modelling approaches for such complex fluid dynamics and nanofluid transport phenomena can be found in Ramesh et al. [42].

To the best knowledge of the authors, the simultaneous effects of Casson rheology, nanoparticle transport, viscous dissipation, thermal radiation, chemical reaction, velocity slip, electromagnetic forces, and non-Darcy porous resistance remains unexplored for flow over a stretching inclined surface. Most existing studies isolate only a subset of these mechanisms, which limits their applicability to real engineering systems where multiple transport phenomena interact simultaneously. This configuration is particularly relevant to advanced thermal and energy systems where surface geometry, microscale slip, and porous resistance play critical roles. The present study is to investigate the unified effects of the radiative and viscous dissipative magnetohydrodynamic flow of a chemically reacting Casson nanofluid over an inclined slippery stretching surface embedded in a non-Darcy porous medium. The concurrent consideration of non-Newtonian Casson rheology, nanoparticle-enhanced heat transfer, magnetic field control, surface slip, chemical reaction, and inertial porous medium effects provides a more realistic and comprehensive model for high-temperature industrial, biomedical, and energy-related applications. The results are expected to offer design guidelines for thermal management systems, catalytic surfaces, and energy devices operating under extreme thermophysical conditions.

2 Problem Formulation

The study develops a comprehensive model of radiative and viscous dissipative flow of a chemically reacting MHD Casson nanofluid over a sloping surface with non-Darcian and slip influence. The flow of Casson nanofluid in a permeable medium over an inclined plane is considered steady, laminar, electrically conducting, incompressible and two-dimensional.

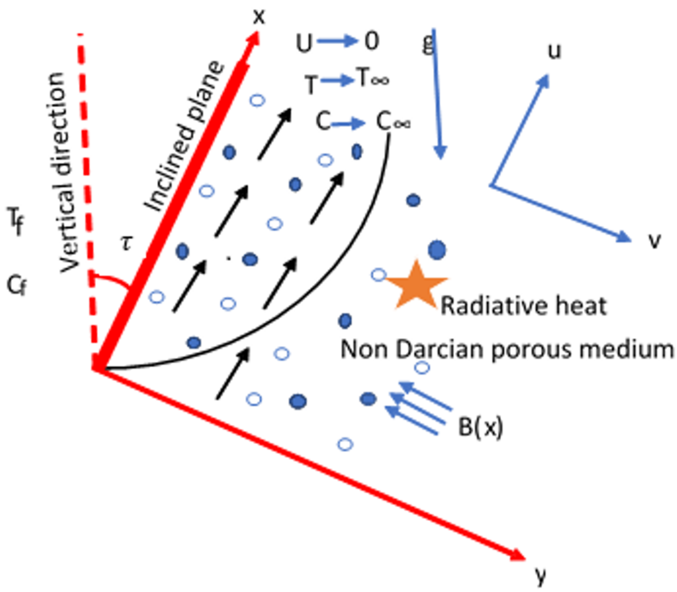

Figure 1. Casson fluid geometry with non darcian penetrable medium.

The x-axis and stretching surface are parallel to each other while y-axis and external transverse magnetic field $B(x) = B_0 x^{\frac{q-1}{2}}$ are normal to the surface as shown in Figure 1. The induced magnetic field is neglected for it is assumed very small. The temperature of the plate surface and free stream are respectively T_f and T_∞ while that of nanoparticle fraction are C_f and C_∞ accordingly. It is assumed that the stretching velocity $U_F(x) = dx^q$ and free stream velocity $U_\infty(x) = 0$, where d is a constant.

The rheological Casson fluid equation following Refs. [37, 38] is:

$$\tau_{ij} = \begin{cases} \left(\mu_B + \frac{p_y}{\sqrt{2\pi}}\right) 2e_{ij}, & \pi > \pi_c \\ \left(\mu_B + \frac{p_y}{\sqrt{2\pi_c}}\right) 2e_{ij}, & \pi < \pi_c \end{cases}$$

where $p_y = \frac{\mu_B \sqrt{2\pi}}{\omega}$ and the respective parameters are defined in the nomenclature section. Considered the above assumptions and following the Boussinesq approximation theory, the governing equations are:

$$\frac{\partial u}{\partial x} + \frac{\partial v}{\partial y} = 0, \tag{1}$$

$$\begin{aligned} & u\frac{\partial u}{\partial x}+v\frac{\partial u}{\partial y} \\ & =\nu\left(1+\frac{1}{\omega}\right)\frac{\partial^2 u}{\partial y^2}-\left(\frac{\sigma B_0^2}{\rho}+\left(1+\frac{1}{\omega}\right)\frac{v}{k_p}\right)u \\ & -\frac{c_f}{\sqrt{k_p}}u^2+g_x\cos[\tau]\left(\beta_t(T-T_\infty)+\beta_c(C-C_\infty)\right), \end{aligned} \tag{2}$$

$$\begin{aligned} u\frac{\partial T}{\partial x}+v\frac{\partial T}{\partial y} &= \alpha\frac{\partial^2 T}{\partial y^2}+\frac{v}{c_p}\left(1+\frac{1}{\omega}\right)\left(\frac{\partial u}{\partial y}\right)^2-\frac{1}{\rho c_p}\frac{\partial q_r}{\partial y} \\ &+\tau^*\left[D_B\frac{\partial c}{\partial y}\frac{\partial T}{\partial y}+\frac{D_T}{T_\infty}\left(\frac{\partial T}{\partial y}\right)^2\right]+\frac{q_0}{\rho c_p}(T-T_\infty) \\ &+\left(\frac{\sigma B_0^2}{\rho c_p}+\left(1+\frac{1}{\omega}\right)\frac{v}{\rho c_p k_p}\right)u^2+\frac{c_f}{\rho c_p\sqrt{k_p}}u^3, \end{aligned} \tag{3}$$

$$u\frac{\partial c}{\partial x}+v\frac{\partial c}{\partial y}=D_B\frac{\partial^2 c}{\partial y^2}+\frac{D_m k_T}{T_m}\frac{\partial^2 T}{\partial y^2}+\frac{D_T}{T_\infty}\frac{\partial^2 T}{\partial y^2}-k(C-C_\infty). \tag{4}$$

with the boundary conditions:

$$\begin{aligned} &\text{at } y=0: \\ &\quad v=v_f=-V(x), \\ &\quad u=U(x)=u_f+u_s+dx^q+N\mu\frac{\partial u}{\partial y}, \\ &\quad T(x)=T_f+T_0\frac{\partial T}{\partial y}, \\ &\quad C(x)=C_f+C_0\frac{\partial C}{\partial y}, \\ &\text{as } y\to\infty: \\ &\quad u\to 0,\quad T\to T_\infty,\quad C\to C_\infty. \end{aligned} \tag{5}$$

where μ is the dynamic viscosity taken as $\left(\mu_B+\frac{p_y}{\sqrt{\pi}}\right)$, $u_s=N_s\mu\frac{\partial u}{\partial y}=N_s\left(\mu_B+\frac{p_y}{\sqrt{\pi}}\right)\frac{\partial u}{\partial y}$, v_f is the mass transfer rate, $v_f>0$ means mass suction while $v_f<0$ denote mass injection.

According to Rosseland's approximation theory [39], the radiative heat flux q_r is taken as

$$q_r=-\frac{4\sigma^*}{3k^*}\frac{\partial T^4}{\partial y}$$

where k^* is the average absorption coefficient, σ^* is the Stefan Boltzmann constant, T^4 is the linear function of temperature and considered sufficiently small within the flow. Hence using the Taylor series expansion to expand T^4 and ignoring higher order terms gives

$$T^4=4T_\infty^3-3T_\infty^4.$$

Following Refs. [36, 37], the stream function and similarity variables are taken as:

$$\begin{aligned} \xi &= \sqrt{\frac{d(q+1)}{2\nu}x^{q-1}}, \\ \psi &= \sqrt{\frac{2d\nu}{q+1}x^{q-1}}f(\xi), \\ u &= \frac{\partial\psi}{\partial y}=dx^q f'(\xi), \\ v &= -\frac{\partial\psi}{\partial x}=-\sqrt{\frac{d\nu(q+1)}{2}x^{q-1}}\left[f(\xi)+\frac{q-1}{q+1}\xi f'(\xi)\right], \\ \theta(\xi) &= \frac{T-T_\infty}{T_f-T_\infty}, \\ \phi(\xi) &= \frac{C-C_\infty}{C_f-C_\infty}. \end{aligned} \tag{6}$$

Implementing equation (6) on the respective dimensional governing equations (1)-(5), yields

$$\begin{aligned} &\left(1+\frac{1}{\omega}\right)f''+ff'-\frac{2q}{q+1}f^2-\frac{2}{q+1}\left[H+\left(1+\frac{1}{\omega}\right)B\right]f' \\ &+f_cf^2+\frac{2}{q+1}\cos[\tau](\gamma\theta+\lambda\phi)=0, \end{aligned}$$

$$\begin{aligned} &\left(1+\frac{4}{3}N\right)\theta''+Prf\theta'+PrEc\left(1+\frac{1}{\omega}\right)\left[f''^2+Bf'^2\right] \\ &+PrEcHBf^2+EcPrf_cf^3+PrNb\phi'\theta'+PrNt\theta'^2 \\ &+\frac{2}{q+1}PrQ\theta=0, \end{aligned} \tag{7}$$

$$\phi''+Scf\phi'+Sc\left(\frac{N_t}{N_b}+Sr\right)\theta''-\frac{2}{q+1}Scg\phi=0. \tag{8}$$

with the boundary conditions

$$\begin{aligned}
&\text{at } \xi = 0: \\
&\quad f'(\xi) = 1 + \lambda_u \left(1 + \frac{1}{\omega}\right) f''(0), \\
&\quad f(\xi) = S, \\
&\quad \theta(\xi) = 1 + \lambda_t \theta'(0), \\
&\quad \phi(\xi) = 1 + \lambda_c \phi'(0), \\
&\text{as } \xi \to \infty: \\
&\quad f(\xi) \to 0, \quad \theta(\xi) \to 0, \quad \phi(\xi) \to 0.
\end{aligned} \tag{9}$$

where

$$\begin{aligned}
&H = \frac{\sigma B_0^2}{d\rho}, \quad B = \frac{v}{dk_p x^{q-1}}, \quad f_c = \frac{c_f x}{\sqrt{k_p}}, \quad \gamma = \frac{G_T}{Re_x^2}, \\
&\lambda = \frac{g_x \beta_t (T_f - T_\infty) x^3}{v^2}, \quad P_r = \frac{v}{\alpha}, \quad E_c = \frac{(dx^q)^2}{C_p (T_f - T_\infty)}, \\
&N = \frac{4\sigma^* T_0^3}{K^* K}, \quad Q = \frac{Q_0}{\rho C_p d x^{q-1}}, \quad S_c = \frac{v}{D_B}, \\
&S_r = \frac{D_m K_T (T_f - T_\infty)}{T_m v (C_f - C_\infty)}, \quad g = \frac{(C_f - C_\infty)}{dx^{q-1}}, \\
&\lambda_u = N_s q x^{q-3} \sqrt{\frac{d(q+1)}{2v}}, \quad S = V_0 \sqrt{\frac{2}{dv(q+1)}}, \\
&\lambda_t = T_0 \sqrt{\frac{d(q+1)}{2v}} x^{q-1}, \quad N_b = \frac{\tau^* D_B (C_f - C_\infty)}{v}, \\
&N_t = \frac{\tau^* D_T (T_f - T_\infty)}{T_\infty v}, \quad G_c = \frac{g_x \beta_c (C_f - C_\infty) x^3}{v^2}, \\
&Re_x = \frac{U_f x}{v}, \quad \lambda_c = C_0 \sqrt{\frac{d(q+1)}{2v}} x^{q-1}.
\end{aligned} \tag{10}$$

3 Flow Characteristics

The flow characteristics is important due to their applications in the field of engineering and Sciences. They are Cf_x, Nu_x and Sh_x, defined as:

$$\begin{aligned}
Cf_x &= \left(\mu_B + \frac{P_y}{\sqrt{2\pi}}\right) \frac{\partial u}{\partial y}\bigg|_{y=0}, \\
Nu_x &= -x \frac{\partial T}{\partial y}\bigg|_{y=0}, \\
Sh_x &= -x \frac{\partial C}{\partial y}\bigg|_{y=0}.
\end{aligned} \tag{11}$$

Using (6) on (12), gives the reduction form of Cf_x, Nu_x and Sh_x where $Re_x = \frac{u_f x}{\nu}$, as:

$$\begin{aligned}
Cf_x \sqrt{\frac{2}{1+q}} Re_x &= \left(1 + \frac{1}{\omega}\right) f'(0), \\
\frac{Nu_x}{\sqrt{\frac{1+q}{2}}} Re_x &= -\theta'(0), \\
\frac{Sh_x}{\sqrt{\frac{1+q}{2}}} Re_x &= -\phi'(0).
\end{aligned} \tag{12}$$

4 Method of Solution

Collocation method with MATHEMATICA 11.0 software are used to obtain the solution of equations (7)-(10). The interval $[0, \infty]$ truncated by $[0, L]$ is transformed to the interior $[-1, 1]$ through the mapping:

$$\eta = \frac{2\xi}{L} - 1 \tag{13}$$

Following Refs [40, 41], the respective assumed Legendre polynomial trial function is provided:

$$\begin{aligned}
f(\xi) &\approxeq f_N(\eta) = \sum_{j=0}^{N} a_j p_j(\eta), \\
\theta(\xi) &\approxeq \theta_N(\eta) = \sum_{j=0}^{N} b_j p_j(\eta), \quad \text{for} \quad j = 0, 1, \ldots, N \\
\phi(\xi) &\approxeq \phi_N(\eta) = \sum_{j=0}^{N} c_j p_j(\eta).
\end{aligned} \tag{14}$$

Equation (16) gives the approximate solution of $f(\xi)$, $\theta(\xi)$ and $\phi(\xi)$ where $p_j(\eta)$ is a finite series sum. The generated equations are used to determine the constant a_j, b_j and c_j and obtained the solution for the flow characteristics. The polynomials are orthogonal, giving good stability and spectral accuracy for smooth problems with fewer basis functions.

5 Results and Discussion

The influence of Thermal radiative and viscous dissipative flow of Casson nanofluid over a stretching inclined surface with nth-order chemical reactions through a Forchheimer pervious medium is established in this study. The influence of some selected parameters on the numerical solutions for flow distributions and characteristics are thoroughly explored. In the present analysis, the choice of parameters are Kr = 0.5, $\tau = \frac{\pi}{3}$, Sr = 0.5, Sc = 2.0,

t = 1, Pr = 6.8, B = 0.2, Fc = 1.0, Q = 0.2, Nb = 0.2, Nt = 0.2, S = 0.2, $\lambda_u = \lambda_t = \lambda_c = 0.3$, ω = 0.3, Ec = 0.1, Gr = Gc = 5, Nr = 0.5, M = 0.5, else otherwise stated. (Following [37]). The respective range of parameters are; $1.0 \leq \omega \leq 3.0$, $0.0 \leq \lambda_u = \lambda_t = \lambda_c \leq 0.3$, $0.0 \leq f_c \leq 3.0$, $0.0 \leq Ec \leq 0.15$, $0.0 \leq N \leq 0.5$, $0.5 \leq S \leq 2.0$, $0.1 \leq N_t = N_b \leq 0.3$, $\pi/9 \leq \tau \leq \pi/3$.

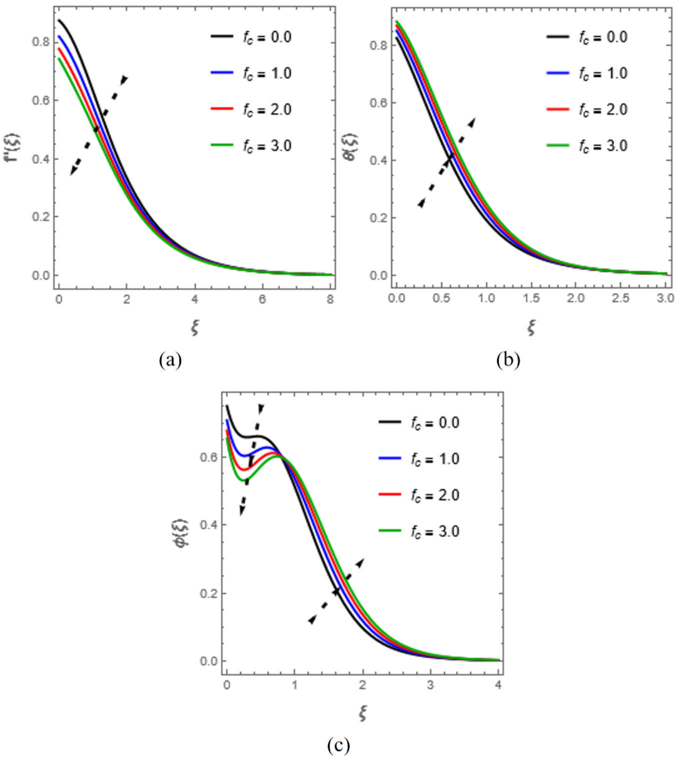

Figure 2. Profile responses to Darcy Forchheimer (Fc) effect. (a) velocity, (b) temperature and (c) concentration.

Figures 2 a, b and c displayed the effects of Darcy Forchheimer (f_c) on velocity, temperature and concentration. In Figure 2a, with increase in fc, there is stronger resistance of the Porous medium as well as inertial drag. This resulted in decrease in fluid velocity due to flow momentum deceleration. This result indicates lower cooling and useful in designing devices involving heat transfer. While, Figure 2b illustrated that high f_c led to increase in the fluid temperature. f_c led to internal friction, eventually, additional heat generated which resulted in hike of the thermal energy. This is useful in industry for efficiency in thermal processing. The effects of f_c on concentration is presented in Figure 2c. Concentration profiles decrease with higher fc due to higher inertial forces, as well as, stronger resistance in the porous medium which increases the transport of solute species or nanoparticles from the boundary thereby causing decrease in concentration up to $\xi = 0.82$, then a reverse trend is noticed. Reduction in concentration can be used to enhance filtration, purification and separation processes.

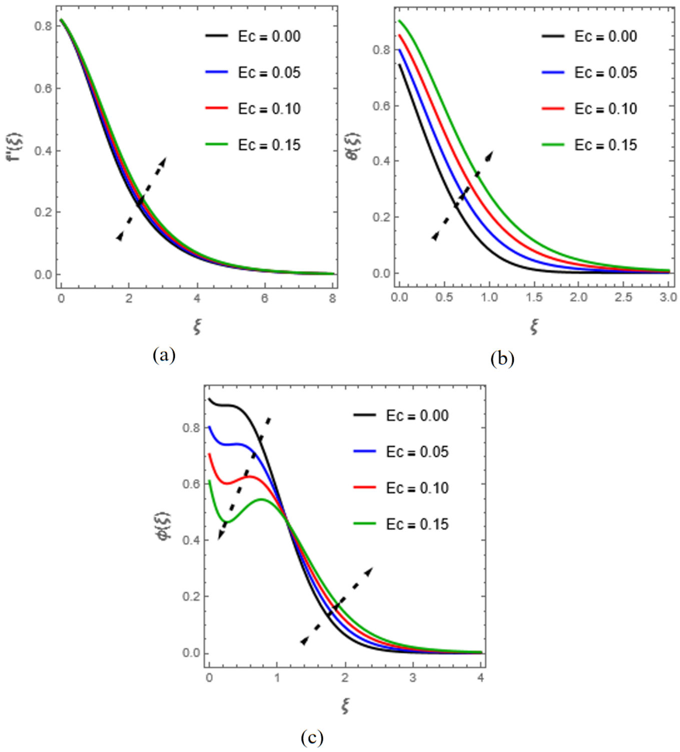

Figure 3. Profile responses to fluid heat dissipation (Ec) effect. (a) velocity, (b) temperature and (c) concentration.

Dissipation effects (E_c) on velocity, temperature and concentration are presented in Figures 3 a, b, and c respectively. Figures 3a depict that high viscous dissipation makes the fluid velocity to increase which implies that fluid viscosity is being reduced by generated heat through internal friction, hence, buoyancy-driven motion is being strengthen. Practically, high velocity has the tendency of enhancing heat removal, as well as, rate of reaction. Likewise, Figures 3b illustrated that rising E_c accelerates the fluid temperature. This indicates that mechanical energy is being converted into heat by frictional forces present in the fluid. Consequently, the fluid viscosity is reduced by this heat generated internally. For industrial purposes, reaction rate, thermal processing and nanoparticles activation can be improved with higher temperature. Though, optimising this, is very important to avoid overheating and material durability reduction. This is useful in designing nanofluid based devices and heat-exchange systems. It is obvious in Figures 3c that increase in E_c decrease the concentration. With higher temperature, solute mobility is enhanced, causing fluid to diffuse rapidly, hence resulting in lower concentration. At $\xi = 1.2$, the trend takes a new turn. This demonstrates a nonlinear effect of internally generated heat on mass transfer.

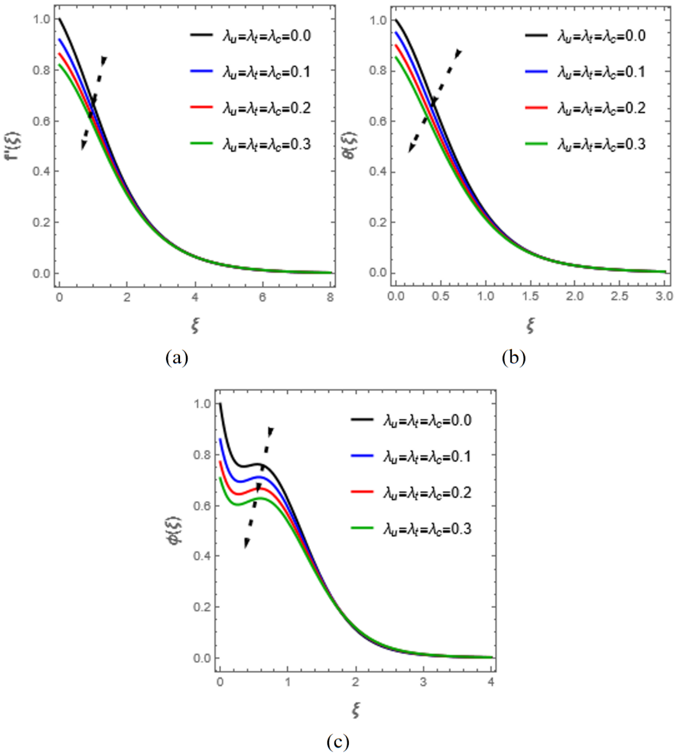

Figure 4. Profile responses to slips effects. (a) (λ_u) on velocity, (b) (λ_t) on temperature and (c) (λ_c) on concentration.

Figures 4 a, b, and c display the influence of slips condition $(\lambda_u, \lambda_t, \lambda_c)$ on velocity, temperature and concentration respectively. In Figure 4a, the fluid witness declined momentum as a result of increase in slips. With higher slips, the speed of the fluid generally is slow down particularly near the boundary. Practically, cooling efficiency is reduced by lower velocity, this requires adjustments in thermal devices and equipment for nanofluid-based processing. Similarly, Figure 4b reveals that higher slips slow down the temperature of the fluid. This result shows that Casson nanofluid in the presence of non-Darcian conditions with MHD experience reduction in the thermal energy retention as a result. It is observed in Figure 4c that increase in slips resulted in decline in fluid concentration. The species convect and diffuse freely, limiting accumulation close to the wall. With lower concentration, filtration, mixing efficiency and purification can be improved.

Figures 5 a, b, and c show effects of inclination angle (τ) on velocity, temperature and concentration profiles respectively. In Figure 5a, velocity decelerated due to increase in τ. This happened as a result of gravitational force component being reduced due to steeper surface. Decline in velocity can decelerate efficiency of heat

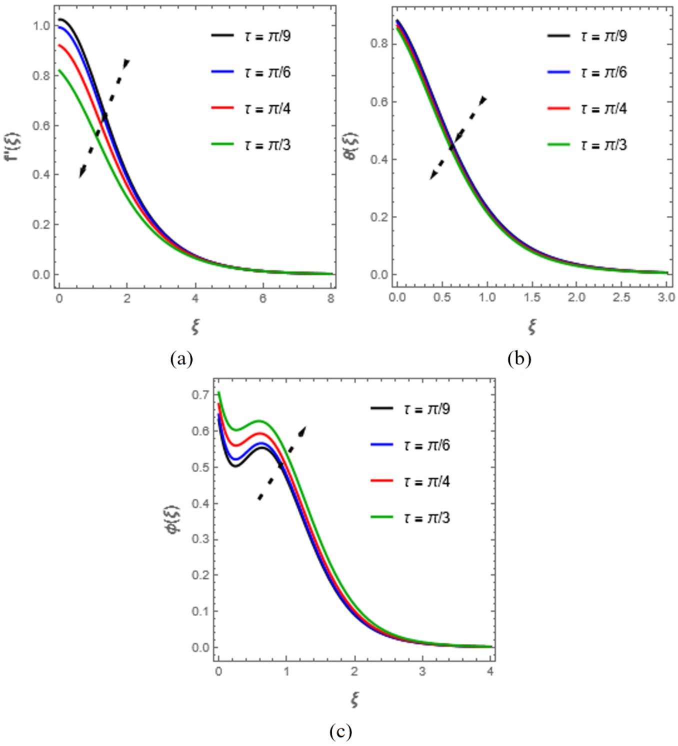

Figure 5. Profile responses to geometrical inclination(τ) effect. (a) velocity, (b) temperature and (c) concentration.

and mass transfer, decrease coating and mixing rates that is important in an inclined channel. Therefore, inclination optimisation is necessary for attaining desire flow and thermal efficiency. Figure 5b shows that increase in τ make the temperature of the fluid to decline. This result of decline velocity via steeper surface cause the convective heat transport to decelerate and thermal energy in the boundary layer to decrease. Thermal profile and process efficiency can be balanced by careful design of inclination. In Figure 5c, it is observed that concentration accelerate due to increase in inclination. This occurs as a result of decline in flow velocity via a steeper surface causing convective transport of nanoparticles from boundary layer, leading to accumulation. This result can be used to balance accumulation and transport in mass transfer of nanofluid-based.

The effect of thermal radiation (N) on velocity, temperature and concentration is displayed in Figures 6 a, b and c respectively. It is observed in Figure 6a that a rise in N makes the velocity profiles to increase. This effect is as a result of radiative heating leads to increase in fluid temperature, decline in viscosity of the fluid, thereby improving flow cause by buoyancy force via inclined surface. Therefore, in the boundary layer, momentum transport is strengthen as a result. Practically,

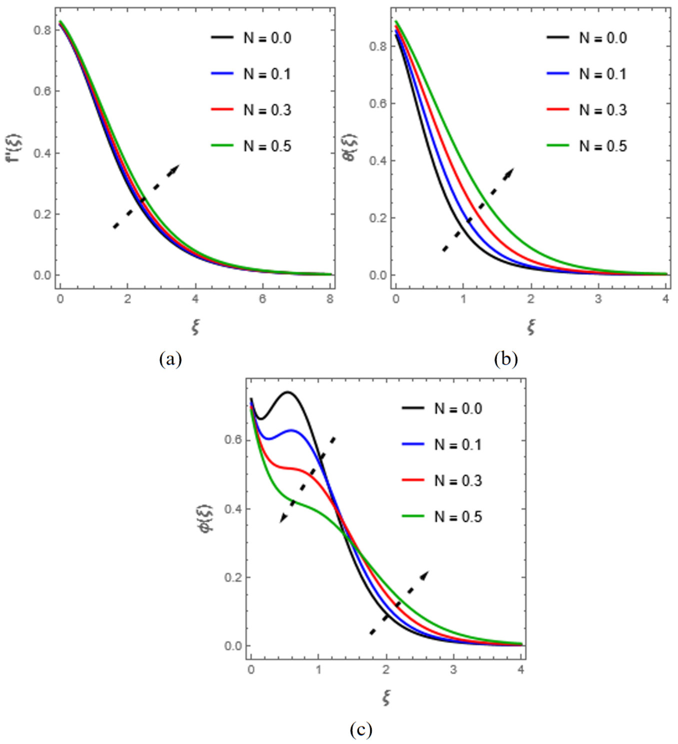

Figure 6. Profile responses to thermal radiation (N) effect. (a) velocity, (b) temperature and (c) concentration.

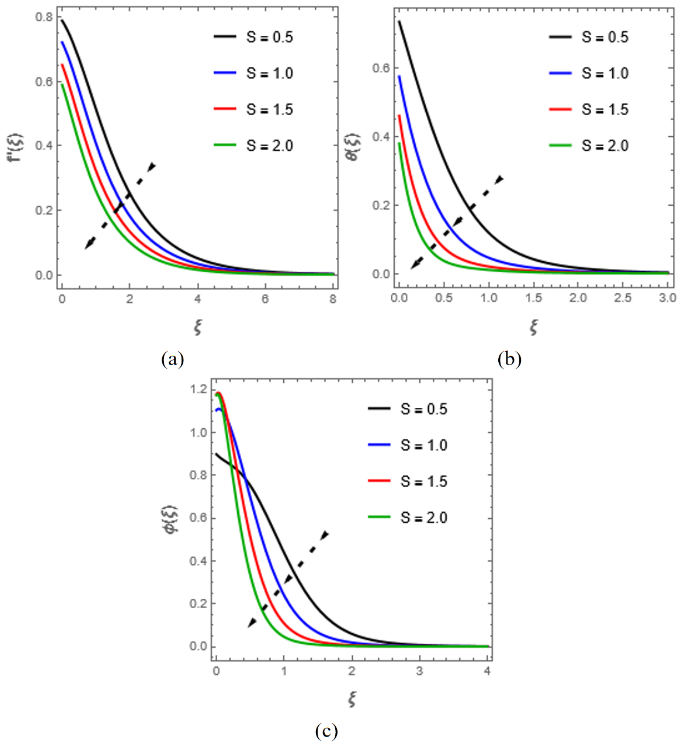

Figure 7. Profile responses to suction (S) effect. (a) velocity, (b) temperature and (c) concentration.

efficiency of heat transfer can be improved with higher velocity. Figure 6b, an increase in N cause the fluid temperature to rise. This is due to the fact that Casson nanofluid is heated directly by radiative energy. Thus, internal energy is improved, there is decline in the fluid viscosity and finally, convective transport is strengthening via inclined surface. This result is useful in designing nanofluid-based devices through thermal management. On the other hand, increase in N lead to decrease in concentration profile up to $\xi = 1.42$, then new trend is observed in Figure 6c. This situation indicates a nonlinear behaviour of mass transport due to radiative heating.

Figures 7a, b and c depict the influence of suction (S) on velocity, temperature and concentration respectively. It is illustrated in Figure 7a that velocity profiles decrease with higher suction. This happened because the momentum of the boundary layer decline by removing fluid via the surface, hence, the flow is slowed down. This result is useful in particle improvement or removal of contaminant. Likewise, in Figure 7b, temperature is slowed down by higher suction. This is as a result of removal of fluid at the surface which decreases the thermal energy. Overheating can be prevented and cooling efficiency can be improved with lower temperatures. Hence, suction optimisation is necessary for thermal management systems involving nanofluid for optimal temperature distribution. Furthermore, Figure 7c reveal that increasing suction has the tendency of declining the concentration profiles. This decline in concentration is due to the fact that boundary layer accumulation is reduced as a result of fluid removal from the surface.

Table 1. Results comparison for $-f'(0)$ and $-\theta'(0)$ with previous studies.

q	Ref. [36]		Ref. [30]		Present results	
	$-f'(0)$	$-\theta'(0)$	$-f'(0)$	$-\theta'(0)$	$-f'(0)$	$-\theta'(0)$
0.0	0.627556	–	0.627556	–	0.627556	–
0.2	0.7668	0.6102	0.766838	0.610203	0.766838	0.610121
0.5	0.8896	0.5949	0.889545	0.595204	0.889545	0.59516
1.0	1.0	–	1.000001	–	1.0	0.581961
3.0	1.1486	0.5647	1.148594	0.564670	1.14859	0.564667
10	1.2349	0.5549	1.234876	0.554890	1.23487	0.554892
100	1.2768	–	1.276775	–	1.27677	0.55022

Table 1 presents a good qualitative agreement with previously reported experimental studies of [29, 35], on MHD flow damping, nanofluid heat transfer and radiative–dissipative effects in non-Newtonian fluids. The observed trends in velocity, temperature, and concentration profiles under magnetic field, thermal

Table 2. Computational results of the flow characteristics when Pr=1, for selected parameters.

Parameter	Value	$-\left(1+\frac{1}{\omega}\right)f'(0)$	$-\left(1+\frac{4}{3}N\right)\theta'(0)$	$\phi'(0)$
	0.5	0.417497	0.155165	0.468372
H	1.0	0.445027	0.151062	0.469299
	1.5	0.469188	0.147276	0.470209
	0.5	0.417494	0.155165	0.468372
Ec	1.0	0.413550	0.124817	0.486804
	1.5	0.409757	0.095557	0.504478
	0.1	0.417497	0.155165	0.468372
Nt	0.2	0.413676	0.156474	0.465442
	0.3	0.409866	0.157590	0.462255
	0.1	0.417497	0.155165	0.468372
Nb	0.2	0.418880	0.151242	0.471089
	0.3	0.419121	0.148644	0.472293
	1.0	0.417497	0.155165	0.468372
ω	2.0	0.447721	0.155953	0.465543
	3.0	0.460162	0.156081	0.464562
	0.1	0.429211	0.226061	0.428855
Q	0.2	0.424020	0.194497	0.446653
	0.3	0.417497	0.155165	0.468372
	0.5	0.417497	0.155165	0.468372
g	1.0	0.425955	0.151297	0.525554
	1.5	0.430996	0.149074	0.562356
	1.0	0.417497	0.155165	0.468372
N	2.0	0.408419	0.127549	0.477005
	3.0	0.404455	0.117670	0.479116
	0.3	0.401906	0.161095	0.360298
Sc	0.6	0.417497	0.155165	0.468372
	0.9	0.425432	0.153304	0.537492

radiation, viscous dissipation, and chemical reaction effects are physically consistent with established experimental findings, confirming the validity of the model.

The comparative analysis for different values of stretching sheet index parameter (q), on the skin friction and Nusselt number is carried out in the Table 1 when the embedded parameters are set as:

$$
\begin{aligned}
H &= Ec - B = Fc - \lambda u = \lambda t = \lambda c = Sc - \tau \\
&= Sr = Q = Nt = Nb = g = \gamma = \lambda = S = N = 0, \\
Pr &= n = 1, \quad \omega = \infty.
\end{aligned}
$$

Therefore, the agreement reinforcing the motivation behind the objectives of the study.

Table 2 highlight the effects of the selected parameters on the flow characteristics for the respective parameters variation. It is observed that skin friction increases with H, Nb, ω, g and Sc, where a decrease is noticed with higher values of Ec, Nt, Q and N. A lower wall temperature is observed as H, Ec, Nb, Q, g, N and Sc increases, while higher wall temperatures are associated with increasing Nt and ω. The Sherwood number generally shows a contrasts behaviour to that of the Nusselt number.

6 Conclusion

This study investigate radiative and viscous dissipation on chemically reacting flow of MHD Casson nanofluid over an inclined slippery stretching surface in a non-Darcian medium shows the relationship between the fluid properties in the presence of porous medium effects. The work points out the combined effects of thermal radiation, magnetic forces, surface slip, viscous dissipation, inclination and suction on the behaviour of the boundary layer. The knowledge of these coupled impacts is necessary for flow patterns prediction, optimisation of heat and mass transfer, improvement in nanofluid-based systems performance in applications involving chemical reactions, radiative heating, and porous media. The results reveal valuable intuition about advanced chemical and thermal processes design and control. The following are the major findings and implications:

1. Darcy Forchheimer: decelerate velocity profiles; affects thermal and concentration distributions as a result of higher inertial and resistive impacts.
2. Viscous dissipation: improves velocity and temperature; concentration either accelerates or decelerates based on thermo-diffusion.
3. Thermal radiation: improves temperature and the flow; transforms solute profile.
4. Velocity, thermal and concentration slips: decline boundary layer Velocity, as well as, temperature; influence concentration distributions and mass transport.
5. Suction: Reduce concentration, temperature, and velocity through thinning boundary layers.

Finally, the results can be used for optimising reactors, heat exchangers, cooling systems, and filtration processes. This gives insight into coupled MHD, viscous dissipative, radiative and non-Darcian medium impacts in a chemically reacting flow in modelling and design of engineering advanced systems which provides a more realistic and comprehensive model for high-temperature industrial, biomedical, and energy-related applications. This study can be extended by considering horizontal or vertical geometry with different non-Newtonian fluid.

Data Availability Statement

Data will be made available on request.

Funding

This work was supported without any funding.

Conflicts of Interest

The authors declare no conflicts of interest.

AI Use Statement

The authors declare that no generative AI was used in the preparation of this manuscript.

Ethical Approval and Consent to Participate

Not applicable.

References

[1] Hussain, T., Shehzad, S. A., Hayat, T., & Alsaedi, A. (2015). Hydromagnetic flow of third grade nanofluid with viscous dissipation and flux conditions. *AIP Advances*, 5(8). [CrossRef]

[2] Nasir, M., Kausar, M. S., Waqas, M., Beg, O. A., & Khan, W. A. (2025). Computational analysis of magnetized Casson liquid stretching flow adjacent to a porous medium with Joule heating, stratification, multiple slip and chemical reaction aspects. *Numerical Heat Transfer, Part A: Applications, 86*(13), 4464-4486. [CrossRef]

[3] Kiyani, M. Z., Hayat, T., Ahmad, I., & Alsaedi, A. (2019). Chemical reaction effectiveness in non-Darcian nanofluid radiated flow considering entropy generation. *International Journal of Numerical Methods for Heat & Fluid Flow, 29*(9), 3535-3556. [CrossRef]

[4] Nadeem, S., Haq, R. U., Akbar, N. S., & Khan, Z. H. (2013). MHD three-dimensional Casson fluid flow past a porous linearly stretching sheet. *Alexandria Engineering Journal, 52*(4), 577-582. [CrossRef]

[5] Hussanan, A., Zuki Salleh, M., Tahar, R. M., & Khan, I. (2014). Unsteady boundary layer flow and heat transfer of a Casson fluid past an oscillating vertical plate with Newtonian heating. *PloS one, 9*(10), e108763. [CrossRef]

[6] Akolade, M. T., Adeosun, T. A., & Olabode, J. O. (2021). Influence of thermophysical features on MHD squeezed flow of dissipative casson fluid with chemical and radiative effects. *Journal of Applied and Computational Mechanics, 7*(4), 1999-2009. [CrossRef]

[7] Oyekunle, T. L., Akolade, M. T., & Agunbiade, S. A. (2021). Thermal-diffusion and Diffusion-thermo effects on heat and mass transfer in chemically reacting MHD Casson nanofluid with viscous dissipation. *Applications and Applied Mathematics: An International Journal (AAM), 16*(1), 39.

[8] Aroloye, S. J., Fenuga, O. J., Abiala, I. O., & Odesola, A. S. (2024). Mhd Casson nanofluid flow with viscous dissipation, chemical reaction and thermal radiation subjected to convective boundary conditions. *Unilag Journal of Mathematics and Applications, 4*(1), 8-20.

[9] Varatharaj, K., Tamizharasi, R., Sivaraj, R., & Vajravelu, K. (2024). Simulation of MHD-Casson hybrid nanofluid dynamics over a permeable stretching sheet: effects of heat transfer and thermal radiation. *Journal of Thermal Analysis and Calorimetry, 149*(15), 8693-8711. [CrossRef]

[10] Buongiorno, J. (2006). Convective transport in nanofluids. *Journal of Heat Transfer, 128*(3), 240–250. [CrossRef]

[11] Kuznetsov, A. V., & Nield, D. A. (2010). Natural convective boundary-layer flow of a nanofluid past a vertical plate. *International Journal of Thermal Sciences, 49*(2), 243-247. [CrossRef]

[12] Gangadharaiah, Y. H., Manjunatha, N., Reddy, M. G., Alghafli, M. A., Ayoob, I., & Mlaiki, N. (2025). Influence of internal heat source on penetrative convection in a dual-component hybrid nanofluid layer. *Results in Engineering*, *27*, 105913. [CrossRef]

[13] Yusuf, A., Bhatti, M. M., & Ellahi, R. (2025). Thermal and sensitivity analysis on regularized curved solar panels using non-Newtonian quaternary hybrid nanofluids: Applications in solar collectors. *Journal of the Indian Chemical Society*, 102256. [CrossRef]

[14] Umar, M., Sabir, Z., Imran, A., Wahab, A. H., Shoaib, M., & Raja, M. A. Z. (2020). The 3-D flow of Casson nanofluid over a stretched sheet with chemical reactions, velocity slip, thermal radiation and Brownian motion. *Thermal Science*, *24*(5 Part A), 2929-2939. [CrossRef]

[15] Islam, M. R., Biswas, R., Hasan, M., Afikuzzaman, M., & Ahmmed, S. F. (2024). Modeling of MHD casson fluid flow across an infinite vertical plate with effects of brownian, thermophoresis, and chemical reactivity. *Arabian Journal for Science and Engineering*, *49*(8), 11139-11156. [CrossRef]

[16] Oyekunle, T. L., Akolade, M. T., Agunbiade, S. A., & Adeniran, P. O. (2024). MHD Stagnation Point Flow of Nanofluid with Buoyancy Effect through a Porous Shrinking Sheet. *Applications & Applied Mathematics*, *19*(1), 1-15. https://digitalcommons.pvamu.edu/aam/vol19/iss1/7/

[17] Idowu, A. S., Akolade, M. T., Oyekunle, T. L., & Abubakar, J. U. (2021). Nonlinear convection flow of dissipative Casson nanofluid through an inclined annular microchannel with a porous medium. *Heat Transfer*, *50*(4), 3388-3406. [CrossRef]

[18] Manjunatha, N., Reddy, M. G., Aloqaily, A., Aljohani, S., Reddy, A. R., Ali, F., & Mlaiki, N. (2025). Radiation effects on rotating system free convective nanofluid unsteady flow with heat source and magnetic field. *Partial Differential Equations in Applied Mathematics*, *13*, 101083. [CrossRef]

[19] Yusuf, A., & Bhatti, M. M. (2026). Coupled nonthermal plasma and photocatalytic surface reactions in mass-based ZnO-Au/water hybrid nanofluid flow. *International Journal of Heat and Fluid Flow*, *117*, 110087. [CrossRef]

[20] Elelamy, A. F., Elgazery, N. S., & Ellahi, R. (2020). Blood flow of MHD non-Newtonian nanofluid with heat transfer and slip effects: application of bacterial growth in heart valve. *International Journal of Numerical Methods for Heat & Fluid Flow*, *30*(11), 4883-4908. [CrossRef]

[21] Ishaq, M., Khan, S. U., Garalleh, H. A., Sowayan, A. S., & Tlili, I. (2025). Thermal performance of casson hybrid nanofluid with radiative effects and convective conditions: applications to energy systems and industrial heat transfer. *Multiscale and Multidisciplinary Modeling, Experiments and Design*, *8*(2), 141. [CrossRef]

[22] Usman, M., Areshi, M., Khan, N., & Eldin, M. S. (2023). Revolutionizing heat transfer: exploring ternary hybrid nanofluid slip flow on an inclined rotating disk with thermal radiation and viscous dissipation effects. *Journal of Thermal Analysis and Calorimetry*, *148*(17), 9131-9144. [CrossRef]

[23] Gebhart, B. (1962). Effects of viscous dissipation in natural convection. *Journal of Fluid Mechanics*, *14*(2), 225-232. [CrossRef]

[24] Muduly, M. M., Rath, P. K., Kar, P., & Swain, K. (2022). Effects of Joule heating and viscous dissipation on Casson nanofluid flow over a stretched sheet with chemical reaction. *Journal of Computational Applied Mechanics*, *53*(4), 478-493. [CrossRef]

[25] Basha, H. (2024). Dynamics of chemically reactive magnetized Casson nanofluid flow over a sensor surface under joule heating and viscous dissipation effects. *BioNanoScience*, *14*(1), 241-267. [CrossRef]

[26] Aziz, A. (2009). A similarity solution for laminar thermal boundary layer over a flat plate with a convective surface boundary condition. *Communications in Nonlinear Science and Numerical Simulation*, *14*(4), 1064-1068. [CrossRef]

[27] Dero, S., Mohd Rohni, A., & Saaban, A. (2020). Effects of the viscous dissipation and chemical reaction on Casson nanofluid flow over the permeable stretching/shrinking sheet. *Heat Transfer*, *49*(4), 1736-1755. [CrossRef]

[28] Manjunatha, N., & Sumithra, R. (2019). Effects of Non-uniform Temperature Gradients on Triple Diffusive Surface Tension Driven Magneto Convection in a Composite Layer. *Universal Journal of Mechanical Engineering*, *7*(6), 398-410. [CrossRef]

[29] Cui, J., Jan, A., Farooq, U., Hussain, M., & Khan, W. A. (2022). Thermal analysis of radiative Darcy–Forchheimer nanofluid flow across an inclined stretching surface. *Nanomaterials*, *12*(23), 4291. [CrossRef]

[30] Bejawada, S. G., Reddy, Y. D., Jamshed, W., Nisar, K. S., Alharbi, A. N., & Chouikh, R. (2022). Radiation effects on MHD Casson fluid flow over an inclined non-linear surface with chemical reaction in a Forchheimer porous medium. *Alexandria Engineering Journal*, *61*(10), 8207-8220. [CrossRef]

[31] Gangadharaiah, Y. H., Manjunatha, N., & Mebarek-Oudina, F. (2024). The variable viscosity and variable gravity field on the onset of convective motion in a porous layer with throughflow. *Mathematical Modeling and Computing*, *11*(1), 19–26. [CrossRef]

[32] Narayanappa, M., Balaji, V. K., Munirathnam, L., & Ramakrishna, S. (2025). Influence of Local Thermal Nonequilibrium and Thermal Gradients on Magneto-Darcy-Rayleigh-Bénard Convective Stability With Heat Generation. *Heat Transfer*, *54*(8), 5260-5275. [CrossRef]

[33] Nield, D. A., & Bejan, A. (2006). *Convection in porous*

media. New York, NY: Springer New York.

[34] Choudhary, S., Mehta, R., Sharma, R., & Ahmad, H. (2025). Numerical analysis on MHD heat transfer of Casson hybrid nanofluid (Cu-Al2O3/H2O) flow across an inclined moving plate in presence of radiation. *Canadian Journal of Physics*, *103*(9), 846-859. [CrossRef]

[35] Kumari, P. S., Ibrahim, S. M., Kumar, P. V., & Lorenzini, G. (2025). Multiple Slips Boundary Layer Flow of Chemically MHD Casson Nanofluid via Homotopic Procedure with Heat Source and Radiation Impacts over an Exponentially Inclined Stretched Surface. *International Journal of Heat & Technology*, *43*(3). [CrossRef]

[36] Ullah, I., Shafie, S., & Khan, I. (2017). Effects of slip condition and Newtonian heating on MHD flow of Casson fluid over a nonlinearly stretching sheet saturated in a porous medium. *Journal of King Saud University-Science*, *29*(2), 250-259. [CrossRef]

[37] Sekhar, P. R., Sreedhar, S., Ibrahim, S. M., & Kumar, P. V. (2023). Radiative heat source fluid flow of MHD Casson nanofluid over a non-linear inclined surface with Soret and Dufour effects. *CFD Letters*, *15*(7), 42-60. [CrossRef]

[38] Bhattacharyya, K., Mukhopadhyay, S., & Layek, G. C. (2011). Slip effects on boundary layer stagnation-point flow and heat transfer towards a shrinking sheet. *International Journal of Heat and Mass Transfer*, *54*(1-3), 308-313. [CrossRef]

[39] Brewster, M. Q. (1992). Thermal radiative transfer and properties. John Wiley& sons. *Inc., New York*.

[40] Olagunju, A. S., Joseph, F. L., & Raji, M. T. (2013). Comparative study of the effect of different collocation points on Legendre-Collocation methods of solving second-order boundary value problems. *IOSR Journal of Mathematics*, *7*(2), 35-41.

[41] Güner, A., & Yalçınbaş, S. (2013). Legendre collocation method for solving nonlinear differential equations. *Mathematical and Computational Applications*, *18*(3), 521-530. [CrossRef]

[42] Ramesh, K., Mebarek-Oudina, F., & Souayeh, B. (Eds.). (2024). *Mathematical modelling of fluid dynamics and nanofluids*. Boca Raton, Florida, USA: CRC Press. [CrossRef]